

Supporting Information

Three ring-shaped Zr(IV)-substituted silicotungstates: syntheses, structures and its properties

Zhong Zhang,^a Yue-Lin Wang,^b Yan Liu,^a Sheng-Li Huang,^a and Guo-Yu Yang^{*,a}

^aMOE Key Laboratory of Cluster Science, School of Chemistry and Chemical Engineering, Beijing Institute of Technology, Beijing 100081, China

^bCollege of Science, Inner Mongolia Agricultural University, Hohhot 010018, China

Table S1. Bond valence sum (BVS) calculations of all Zr, W and select O atoms in **1-3**.

Table S2. Selected bond angles (°) of **1-3**.

Table S3. The impact of reaction temperature on the H₂O₂-based oxidation reaction of EPS.

Table S4. The impact of molar amount of catalyst **2** on the H₂O₂-based oxidation reaction of EPS.

Table S5. The impact of reaction time on the H₂O₂-based oxidation reaction of EPS.

Table S6. The impact of molar amount of H₂O₂ on the H₂O₂-based oxidation reaction of EPS.

Table S7. Results for oxygenation of various thioethers with 30% H₂O₂ without catalyst **2** in MeCN.

Fig. S1 IR spectrums of **1-3**.

Fig. S2 The comparisons of PXRD spectra of **1-3** with the simulated X-ray diffraction patterns based on single-crystal structural analysis.

Fig. S3 UV-Vis optical diffuse reflectance spectra and plots of Kubelka-Munk function versus energy E_g (eV) of **1-3**.

Fig. S4 The TG curves of **1-3**.

Fig. S5 (a) The coordination environment of the Zr cations in **1**. (b, c) The {Zr₂} clusters in **1**. (d) View of the 2-D layer formed via the linkers of H-bonds. (d,e) The sql topological net with the double edges in **1**.

Fig. S6 (a, b) The coordination environment of the Zr cations in **2**. (c,d,e,f) The {Zr₂} clusters in **2**.

Fig. S7 (a,b) The {Na₃} and {Na₂} clusters in **2**. (c,d) The structures of cage and double cage.

Fig. S8 (a) View of 1-D {Na₂}_n chain. (b,c) The connected modes of each **3a** and {Na₂}_n chain. (d) View of 3-D framework formed via the linkers of 1D {Na₂}_n chain.

Fig. S9 (a, b) The UV spectra and CVs of **2** were tested in Na₂SO₄/H₂SO₄ buffer solution with different pH. (c, d) The UV spectra and CVs of **2** were detected for seven times per 10 hours.

Fig. S10 (a) CV of **2** (concentration: 1×10⁻³ mol·L⁻¹) in 0.5 mol·L⁻¹ (pH=4.0) Na₂SO₄/H₂SO₄ buffer solution at a scan rate of 100 mV·s⁻¹. (b) CVs of **2** in 0.5 mol·L⁻¹ (pH=4.0) Na₂SO₄/H₂SO₄ buffer solution at different scan rates (from inner to outer plots: 50, 100, 200, 300, 400 and 500 mV·s⁻¹). Inset: the linear relationship between cathodic peak currents (I_{III}) and the scan speed for **2**. The working electrode was glassy carbon, and the reference electrode was Ag/AgCl.

Fig. S11 (a) CVs of **1** and **3** (concentration: 1×10⁻³ mol·L⁻¹) in 0.5 mol·L⁻¹ (pH=4.0) Na₂SO₄/H₂SO₄ buffer solution at a scan rate of 100 mV·s⁻¹.

Fig. S12 (a, b, c) The variation of CVs of **2** (concentration: 1×10⁻³ mol·L⁻¹) in 0.5 mol·L⁻¹ (pH=4.0) Na₂SO₄/H₂SO₄ buffer solution with the amount of different H₂O₂, NaNO₂, and NaBrO₃. Scan speed: 100 mV·s⁻¹.

Fig. S13 (a) CV of {A-α-SiW₉} (concentration: 1×10⁻³ mol·L⁻¹) in 0.5 mol·L⁻¹ (pH=4.0) Na₂SO₄/H₂SO₄ buffer solution. (b) The variation of CVs of {A-α-SiW₉} (concentration: 1×10⁻³ mol·L⁻¹) in 0.5 mol·L⁻¹ (pH=4.0) Na₂SO₄/H₂SO₄ buffer solution with the amount of different H₂O₂. Scan speed: 100 mV·s⁻¹.

Fig. S14 GC trace of the catalytic results for different catalysts on oxidation of EPS. Reactions conditions: EPS (0.5 mmol), 30% H₂O₂ (1.5 mmol), and catalysts (2.5 μmol) in CH₃CN (6 mL) at 80 °C, 3h.

Fig S15. GC trace of the catalytic results for different reactions conditions on oxidation of EPS. Reactions conditions:

(a) EPS (0.5 mmol), 30% H₂O₂ (1.5 mmol), catalyst **2** (0/0.625/1.25/2.5 μmol), CH₃CN (6 mL), 80 °C 3h. (b) EPS (0.5 mmol), 30% H₂O₂ (1.5 mmol), catalyst **2** (2.5 μmol), CH₃CN (6 mL), 80 °C 1/2/3 h. (c) EPS (0.5 mmol), 30% H₂O₂ (0.5/1.0/1.5 mmol), catalyst **2** (2.5 μmol), CH₃CN (6 mL), 80 °C 3h. (d) EPS (0.5 mmol), 30% H₂O₂ (1.5 mmol), catalyst **2** (2.5 μmol), CH₃CN (6 mL), 60/70/80 °C 3h.

Fig S16. GC trace of the catalytic results for oxidation of entries 1 and 3-10. Reactions conditions: entries 1 and 3-10 (0.5 mmol), 30% H₂O₂ (1.5 mmol), and catalyst **2** (2.5 μmol) in CH₃CN (6 mL) at 80 °C, 3h.

Fig. S17 Comparison of IR spectra of the fresh catalyst and the recovered catalyst after the fifth-run catalytic reaction in entry 2.

Fig. S18 Comparison of PXRD patterns of the fresh catalyst and the recovered catalyst after the fifth-run catalytic reaction in entry 2.

Table S1. Bond valence sum (BVS) calculations of all Zr , W and select O Atoms in **1-3**.

1-BVS				2-BVS						3-BVS	
O1	1.12	W17	6.43	O1	1.07	Si2	4.07	W23	6.33	O1	0.99
O2	1.14	W18	6.35	O2	1.21	Si3	3.83	W24	6.03	O2	1.00
O3	1.17	W19	6.31	O3	1.08	Si4	4.16	W25	5.95	O3	1.81
O4	1.21	W20	6.45	O4	0.97	W1	5.92	W26	5.96	O4	0.95
Zr1	4.08			O5	1.98	W2	6.20	W27	6.19	O5	1.14
Zr2	4.10			O6	0.90	W3	6.15	W28	5.88	O6	1.81
Zr3	4.14			O7	0.95	W4	6.13	W29	6.16	O7	0.95
Zr4	4.09			O8	1.18	W5	6.27	W30	5.96	O8	1.78
Si1	3.95			O9	1.14	W6	6.16	W31	6.32	O9	0.95
W1	6.08			O10	0.98	W7	6.17	W32	6.10	B1	2.96
W2	6.22			O11	0.97	W8	6.44	W33	6.00	B2	2.96
W3	6.45			O12	2.01	W9	6.44	W34	6.16	B3	2.75
W4	6.47			O13	1.18	W10	6.22	W35	6.33	Zr1	3.89
W5	6.24			O14	0.95	W11	6.10	W36	6.36	Zr2	3.94
W6	6.48			B1	3.03	W12	6.15	W37	5.96	Si1	4.03
W7	6.47			B2	3.34	W13	6.26	W38	6.29	W1	6.07
W8	6.22			Zr1	4.08	W14	6.15	W39	6.35	W2	6.32
W9	5.75			Zr2	3.85	W15	6.19	W40	6.08	W3	6.10
W10	6.16			Zr3	3.88	W16	6.19			W4	6.15
W11	6.06			Zr4	3.97	W17	6.42			W5	6.16
W12	6.02			Zr5	3.96	W18	6.14			W6	6.15
W13	6.40			Zr6	3.78	W19	6.22			W7	6.43
W14	6.28			Zr7	3.89	W20	6.11			W8	6.20
W15	5.77			Zr8	3.95	W21	6.11			W9	6.11
W16	6.27			Si1	3.95	W22	6.26			W10	6.19

Table S2. Selected bond angles (°) of **1-3**.

1		2				3	
Zr1-O1-Zr4A	113.8(7)	Zr1-O1-Zr8	114.4(9)	Zr5-O8-Zr4	115.3(9)	Zr1-O1-Zr1C	99.3(10)
Zr2-O4-Zr3	111.6(9)	Zr1-O2-Zr8	116.6(9)	Zr6-O10-Zr7	98.6(7)	Zr1-O2-Zr1C	99.4(10)
Zr1-O2-Zr4A	113.1(9)	Zr2-O3-Zr3	100.0(8)	Zr7-O11-Zr6	98.5(7)	Zr1-O3-Zr1C	93.1(10)
Zr2-O3-Zr3	112.2(8)	Zr2-O5-Zr3	95.3(8)	Zr7-O12-Zr6	95.1(7)	Zr2-O5-Zr2A	103.2(10)
		Zr3-O4-Zr2	97.4(8)			Zr2-O6-Zr2A	93.8(9)
		Zr4-O9-Zr5	114.4(9)			Zr2-O8-Zr2A	96.6(10)

Table S3. The impact of reaction temperature on the H₂O₂-based oxidation reaction of EPS.

Entry ^a	Temp. (°C)	Conv. (%)	Selectivity(%) RR'SO / RR'SO ₂	
1	60	19	41	59
2	70	93	89	11
3	80	100	0	100

^aReaction conditions: substrate, 0.5 mmol; H₂O₂, 1.5 mmol; compound **2**, 2.5 μmol; time, 3 h; MeCN, 6 mL.

Table S4. The impact of molar amount of catalyst **2** on the H₂O₂-based oxidation reaction of EPS.

Entry ^a	n(μmol)	Conv(%)	Selectivity(%) RR'SO/RR'SO ₂	
1	0.625	85	28	72
2	1.25	97	17	83
3	2.5	100	0	100

^aReaction conditions: substrate, 0.5 mmol; H₂O₂, 1.5 mmol; temperature, 80 °C; time, 3 h; MeCN, 6 mL.

Table S5. The impact of reaction time on the H₂O₂-based oxidation reaction of EPS.

Entry	Time(h)	Conv(%)	Selectivity(%) RR'SO / RR'SO ₂	
1 ^a	1	85	29	71
2	2	97	10	90
3	3	100	0	100

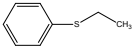
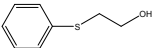
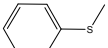
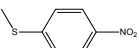
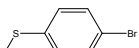
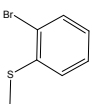
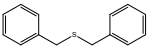
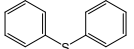
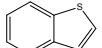
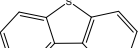
^aReaction conditions: substrate, 0.5 mmol; H₂O₂, 1.5 mmol; compound **2**, 2.5 μmol; temperature, 80 °C; MeCN, 6 mL.

Table S6. The impact of molar amount of H₂O₂ on the H₂O₂-based oxidation reaction of EPS.

Entry	n(mmol)	Conv(%)	Selectivity(%)RR'SO/RR'SO ₂	
1	0.5	49	52	48
2	1.0	85	22	78
3	1.5	100	0	100

^aReaction conditions: substrate, 0.5 mmol; time, 3 h; compound **2**, 2.5 μmol; temperature, 80 °C; MeCN, 6 mL.

Table S7. Results for oxygenation of various thioethers with 30% H₂O₂ without catalyst **2** in MeCN solution.

Entry ^a	Substrate	Time (h)	Temp. (°C)	Conv. (%) ^[a]	Selectivity(%)	
					RR'SO	RR'SO ₂
1		3	80	11	97	3
2		3	80	9	57	43
3		3	80	20	34	66
4		3	80	5	64	36
5		3	80	24	48	52
6		3	80	12	73	27
7		3	80	20	9	97
8		3	80	5	100	0
9		3	80		Trace	
10		3	80		Trace	

^a Reaction conditions: substrate, 0.5 mmol; H₂O₂, 1.5 mmol; temperature, 80 °C; time, 3 h; MeCN, 6 mL.

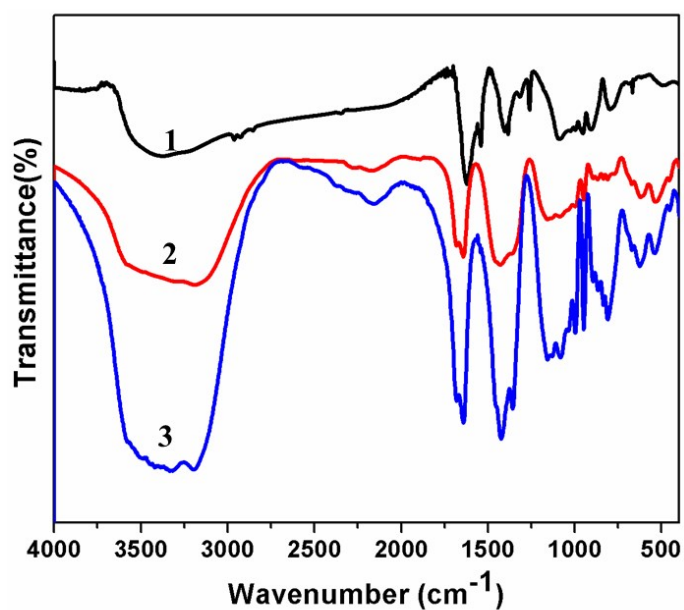


Fig. S1 IR spectra of 1-3.

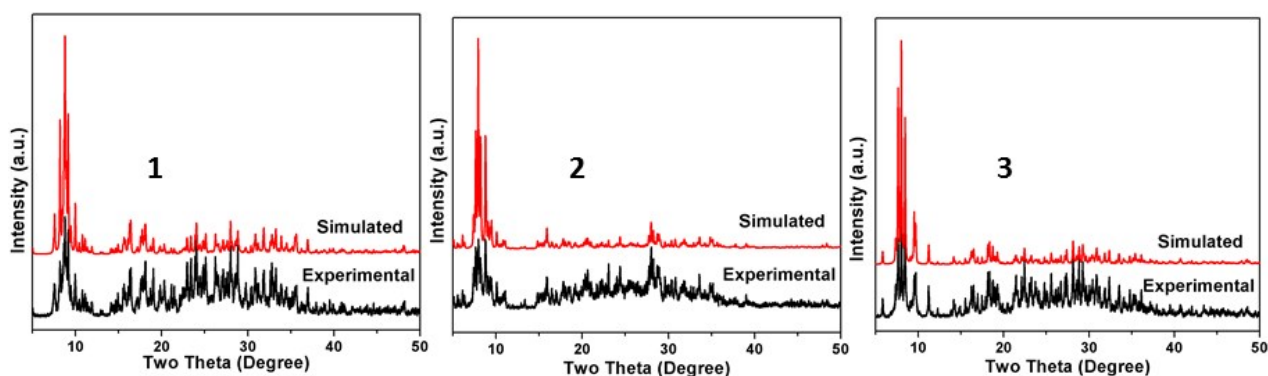


Fig. S2 The comparisons of PXRD spectra of **1-3** with the simulated X-ray diffraction patterns based on single-crystal structural analysis.

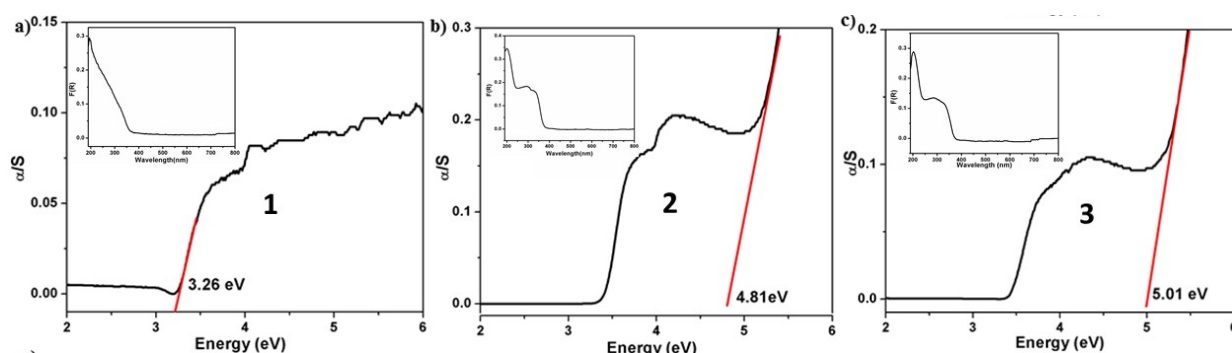


Fig. S3 UV-Vis optical diffuse reflectance spectra and plots of Kubelka-Munk function versus energy E_g (eV) of **1-3**.

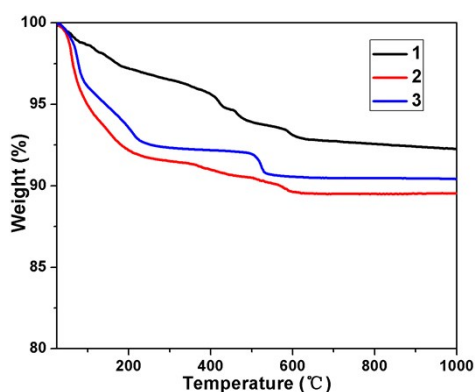


Fig. S4 The TG curves of **1-3**.

The TG curves indicate that two weight loss steps for **1-3** between 25 and 1000 °C (Fig. S4). For **1**, the total weight loss of the first and the second steps, with the combined weight loss of 7.07% (calcd. 6.49%) corresponding to release of eight lattice water molecules, four dap ligands, the dehydration of eight hydroxy groups and the dehydration of sixteen protons; For **2**, the total weight loss of the first and the second steps, with the combined weight loss of 10.50% (calcd. 9.61%) involves in the release of fifty lattice water molecules, the dehydration of twelve hydroxyl groups and the dehydration of seventeen protons; For **3**, the total weight loss of the first and the second steps, with the combined weight loss of 9.52% (calcd. 8.84%) corresponding to release of forty lattice water molecules, the dehydration of eighteen hydroxyl groups and the dehydration of twenty protons. All these analyses reveal that the experimental values are approximately consistent with the theoretical values.

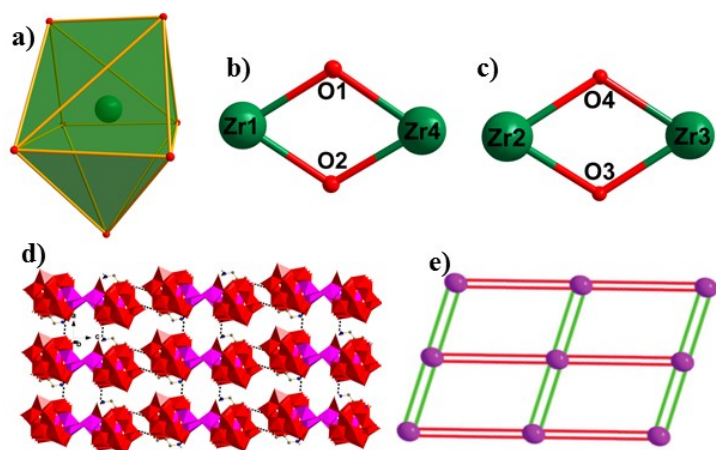


Fig. S5 (a) The coordination environment of the Zr cations in **1**. (b, c) The $\{Zr_2\}$ clusters in **1**. (d) View of the 2-D layer formed via the linkers of H-bonds. (d,e) The sql topological net with the double edges in **1**.

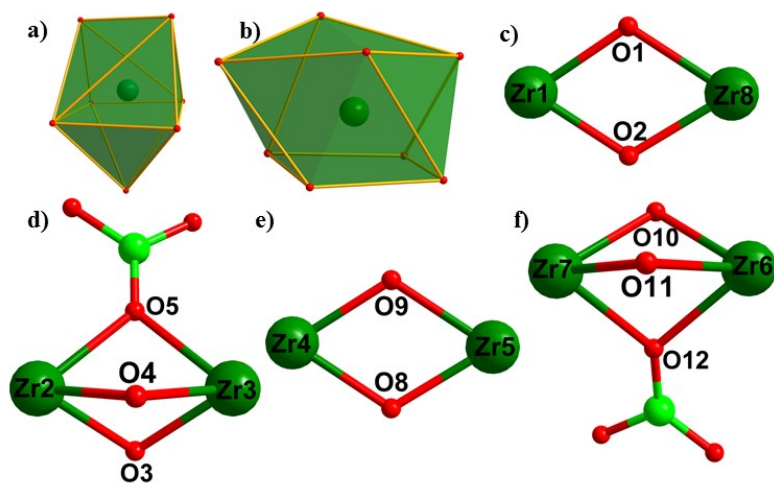


Fig. S6 (a, b) The coordination environment of the Zr cations in **2**. (c,d,e,f) The $\{Zr_2\}/\{Zr_2B\}$ clusters in **2**.

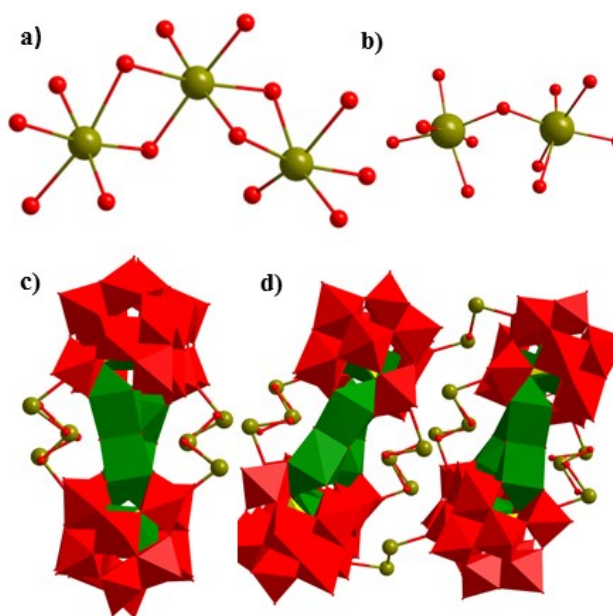


Fig. S7 (a, b) The $\{Na_3\}$ and $\{Na_2\}$ clusters in **2**. (c, d) The structures of cage and double cage.

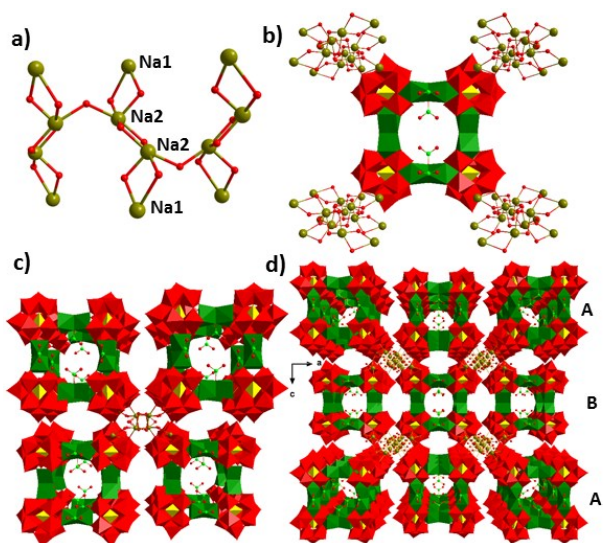


Fig. S8 (a) View of 1-D $\{\text{Na}_2\}_n$ chain. (b,c) The connected modes of each **3a** and $\{\text{Na}_2\}_n$ chain. (d) View of 3-D framework formed via the linkers of 1D $\{\text{Na}_2\}_n$ chain.

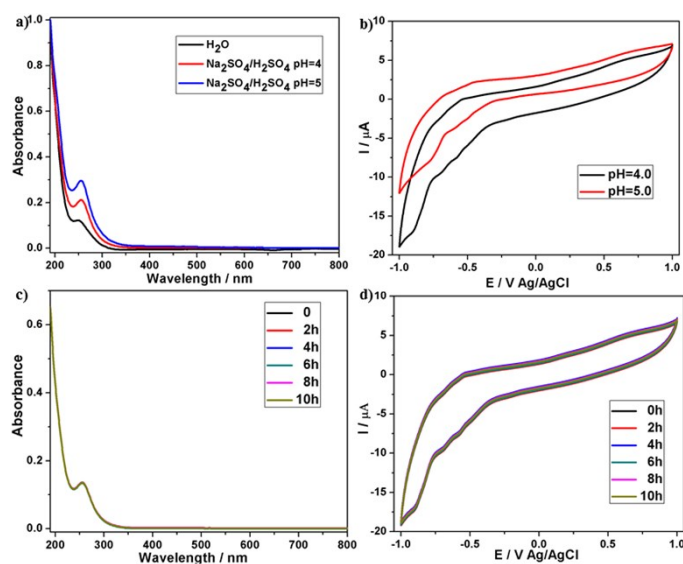


Fig. S9 (a, b) The UV spectra and CVs of **2** were tested in $\text{Na}_2\text{SO}_4/\text{H}_2\text{SO}_4$ buffer solution with different pH. (c, d) The UV spectra and CVs of **2** were detected for seven times per 10 hours.

Cyclic voltammograms (CVs) were recorded on a CS electro-chemical workstation at room temperature. In the experiments, we used twice-distilled water. We used a three-electrode system in which glassy carbon acted as the working electrode, the counter electrode was a platinum gauze, and an Ag/AgCl electrode was used as a reference. The supporting electrolyte for **1-3** was an aqueous solution of $0.5 \text{ mol}\cdot\text{L}^{-1} \text{ Na}_2\text{SO}_4/\text{H}_2\text{SO}_4$.

CV experiments were performed to examine the redox properties of **1-3** in $0.5 \text{ mol}\cdot\text{L}^{-1} \text{ Na}_2\text{SO}_4/\text{H}_2\text{SO}_4$ solution. The tetrameric polyoxoanion clusters in **1-3** are similar and soluble in water, so we selected **2** as an example to survey the stability. The cyclic voltammetric (CV) and UV-vis spectra (UV) of **2** in $0.5 \text{ mol}\cdot\text{L}^{-1} \text{ Na}_2\text{SO}_4/\text{H}_2\text{SO}_4$ solution was recorded at different pH values (Fig. S9). The reproducibility of the spectra from pH 4 to 5 confirms their stability in this pH range. **2** in $0.5 \text{ mol}\cdot\text{L}^{-1}$ (pH=4) $\text{Na}_2\text{SO}_4/\text{H}_2\text{SO}_4$ solution was remained stable for at least 10 h at room temperature in dark surroundings. The CV and UV of this solution were checked six times in 10h, and the CV and UV characteristics of this solution show no obvious changes, indicating that **2** is stable in $0.5 \text{ mol}\cdot\text{L}^{-1}$ (pH = 4.0) $\text{Na}_2\text{SO}_4/\text{H}_2\text{SO}_4$ solution. Using similar method, the electrochemistry property of a large

number of POMs have been investigated for this method.^[1]

The structure of **1-3** are stable in pH = 4.0 0.5M Na₂SO₄/H₂SO₄ buffer solution. Keeping pH = 4.0, from -1.0 to + 1.0 V at a scan rate of 100 mV·s⁻¹, the CV of **1-3** exhibits similar electrochemical behavior (Fig. S10-S11). Therefore, we describe the electrochemical behavior of **2** in detail as example. In the negative region, one oxidation wave (III, E_{pc} = -0.898 V) and two quasi-reversible redox peaks (I (-0.576 V) /I'(-0.546) and II (-0.702 V) /II'(-0.692 V)) are attributed to the W^{VI} center redox. The half-wave potentials E_{1/2} of I/I' and II/II' are -0.561 and -0.696 V and attributed to the redox process of the W centers. Compared with **2**, the CV curve of the {A-α-SiW₉} precursor (Fig. S13a) exhibits a potential shift, which may be resulted from the different ST fragments, extra Zr₂(OH)₂/Zr₂(BO(OH)₂)(OH)₂ clusters, and different negative charges. The peak-current intensities for W^{VI} in **2** redox processes are almost linear to the scan rates with the consistency factor of 0.995, indicating that the redox processes are probably surface-controlled in the specific range of 50-500 mV·s⁻¹ scan rates. In addition, the Zr centers of **1-3** are not observed in our case.

- [1] a) M. Ibrahim, Y. X. Xiang, B. S. Bassil, Y. H. Lan, A. K. Powell, P. D. Oliveira, B. Keita, U. Kortz, *Inorg. Chem.* **2013**, 52, 8399. b) M. Ibrahim, A. Haider, Y. H. Lan, B. S. Bassil, A. M. Carey, R. J. Liu, G. J. Zhang, B. Keita, W. H. Li, G. E. Kostakis, A. K. Powell, U. Kortz, *Inorg. Chem.* **2014**, 53, 5179.

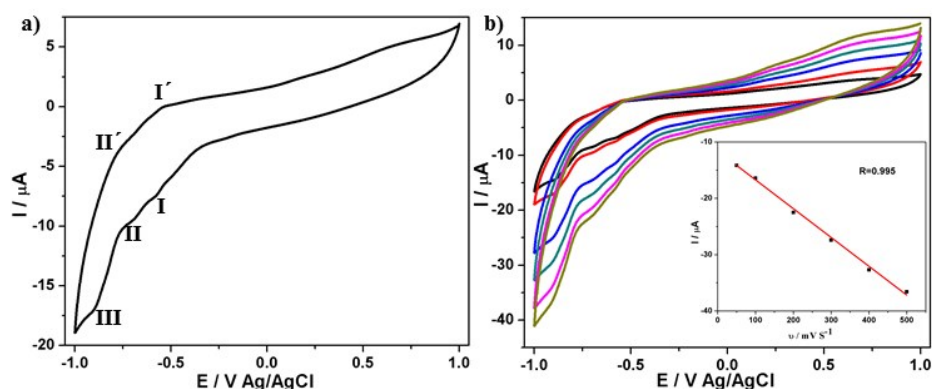


Fig. S10 (a) CV of **2** (concentration: 1×10^{-3} mol·L⁻¹) in 0.5 mol·L⁻¹ (pH=4.0) Na₂SO₄/H₂SO₄ buffer solution at a scan rate of 100 mV·s⁻¹. (b) CVs of **2** in 0.5 mol·L⁻¹ (pH=4.0) Na₂SO₄/H₂SO₄ buffer solution at different scan rates (from inner to outer plots: 50, 100, 200, 300, 400 and 500 mV·s⁻¹). Inset: the linear relationship between cathodic peak currents (III) and the scan speed for **2**. The working electrode was glassy carbon, and the reference electrode was Ag/AgCl.

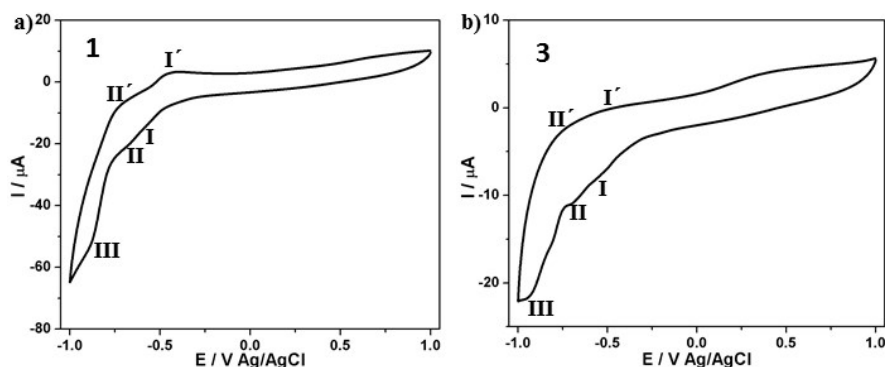


Fig. S11 (a) CVs of **1** and **3** (concentration: 1×10^{-3} mol·L⁻¹) in 0.5 mol·L⁻¹ (pH=4.0) Na₂SO₄/H₂SO₄ buffer solution at a scan rate of 100 mV·s⁻¹.

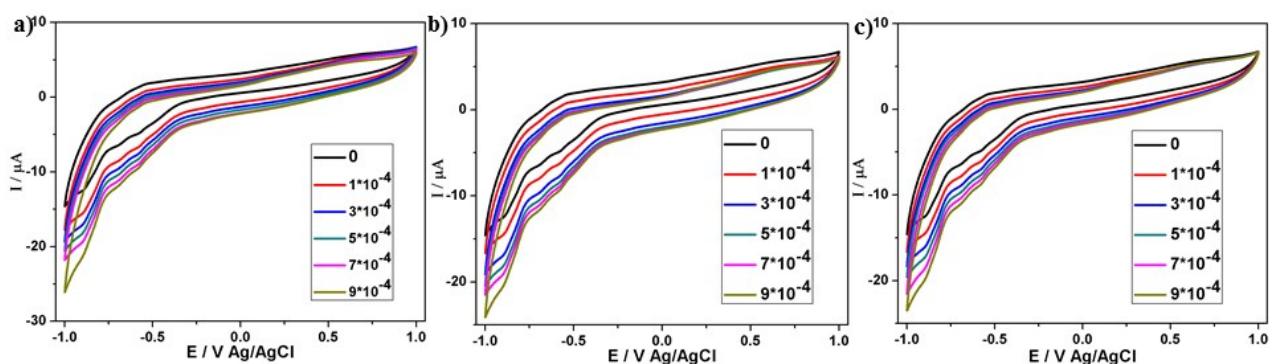


Fig. S12 (a, b, c) The variation of CVs of **2** (concentration: $1 \times 10^{-3} \text{ mol} \cdot \text{L}^{-1}$) in $0.5 \text{ mol} \cdot \text{L}^{-1}$ (pH=4.0) $\text{Na}_2\text{SO}_4/\text{H}_2\text{SO}_4$ buffer solution with the amount of different H_2O_2 , NaNO_2 , and NaBrO_3 . Scan speed: $100 \text{ mV} \cdot \text{s}^{-1}$.

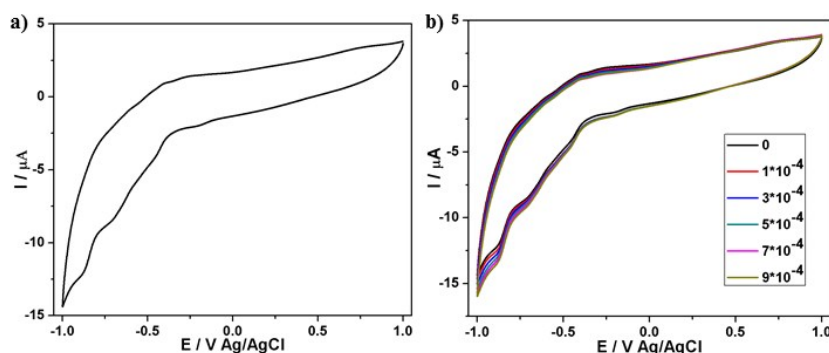


Fig. S13 (a) CV of $\{\text{A-}\alpha\text{-SiW}_9\}$ (concentration: $1 \times 10^{-3} \text{ mol} \cdot \text{L}^{-1}$) in $0.5 \text{ mol} \cdot \text{L}^{-1}$ (pH=4.0) $\text{Na}_2\text{SO}_4/\text{H}_2\text{SO}_4$ buffer solution. (b) The variation of CVs of $\{\text{A-}\alpha\text{-SiW}_9\}$ (concentration: $1 \times 10^{-3} \text{ mol} \cdot \text{L}^{-1}$) in $0.5 \text{ mol} \cdot \text{L}^{-1}$ (pH=4.0) $\text{Na}_2\text{SO}_4/\text{H}_2\text{SO}_4$ buffer solution with the amount of different H_2O_2 . Scan speed: $100 \text{ mV} \cdot \text{s}^{-1}$.

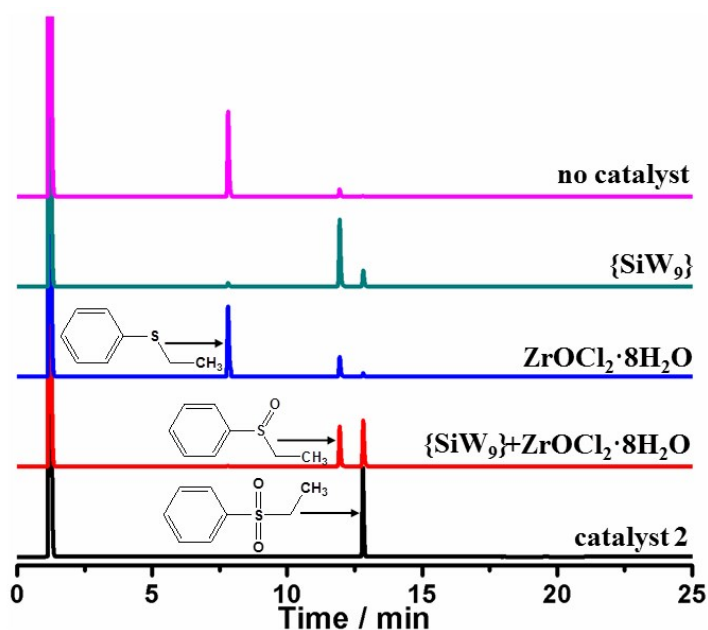


Fig S14. GC trace of the catalytic results for different catalysts on oxidation of EPS. Reactions conditions: MPS (0.5 mmol), 30% H_2O_2 (1.5 mmol), and catalysts (2.5 μmol) in CH_3CN (6 mL) at 80°C , 3h.

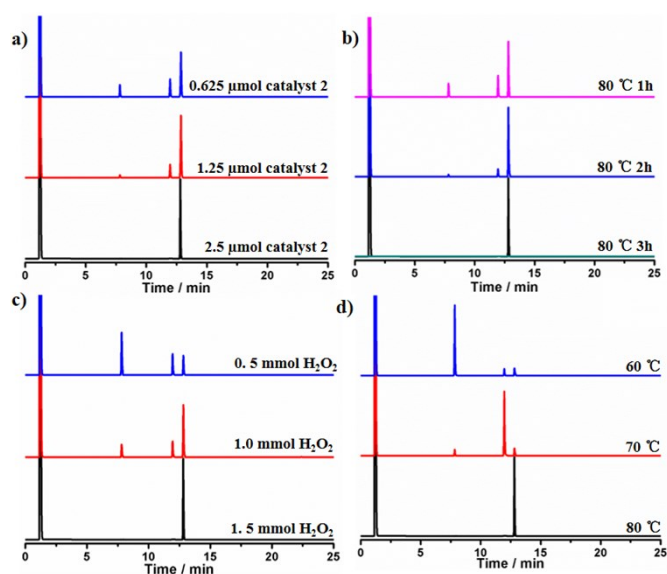


Fig S15. GC trace of the catalytic results for different reactions conditions on oxidation of EPS. Reactions conditions: (a) EPS (0.5 mmol), 30% H₂O₂ (1.5 mmol), catalyst **2** (0/0.625/1.25/2.5 μmol), CH₃CN (6 mL), 80 °C 3h. (b) EPS (0.5 mmol), 30% H₂O₂ (1.5 mmol), catalyst **2** (2.5 μmol), CH₃CN (6 mL), 80 °C 1/2/3 h. (c) EPS (0.5 mmol), 30% H₂O₂ (0.5/1.0/1.5 mmol), catalyst **2** (2.5 μmol), CH₃CN (6 mL), 80 °C 3h. (d) MPS (0.5 mmol), 30% H₂O₂ (1.5 mmol), catalyst **2** (2.5 μmol), CH₃CN (6 mL), 60/70/80 °C 3h.

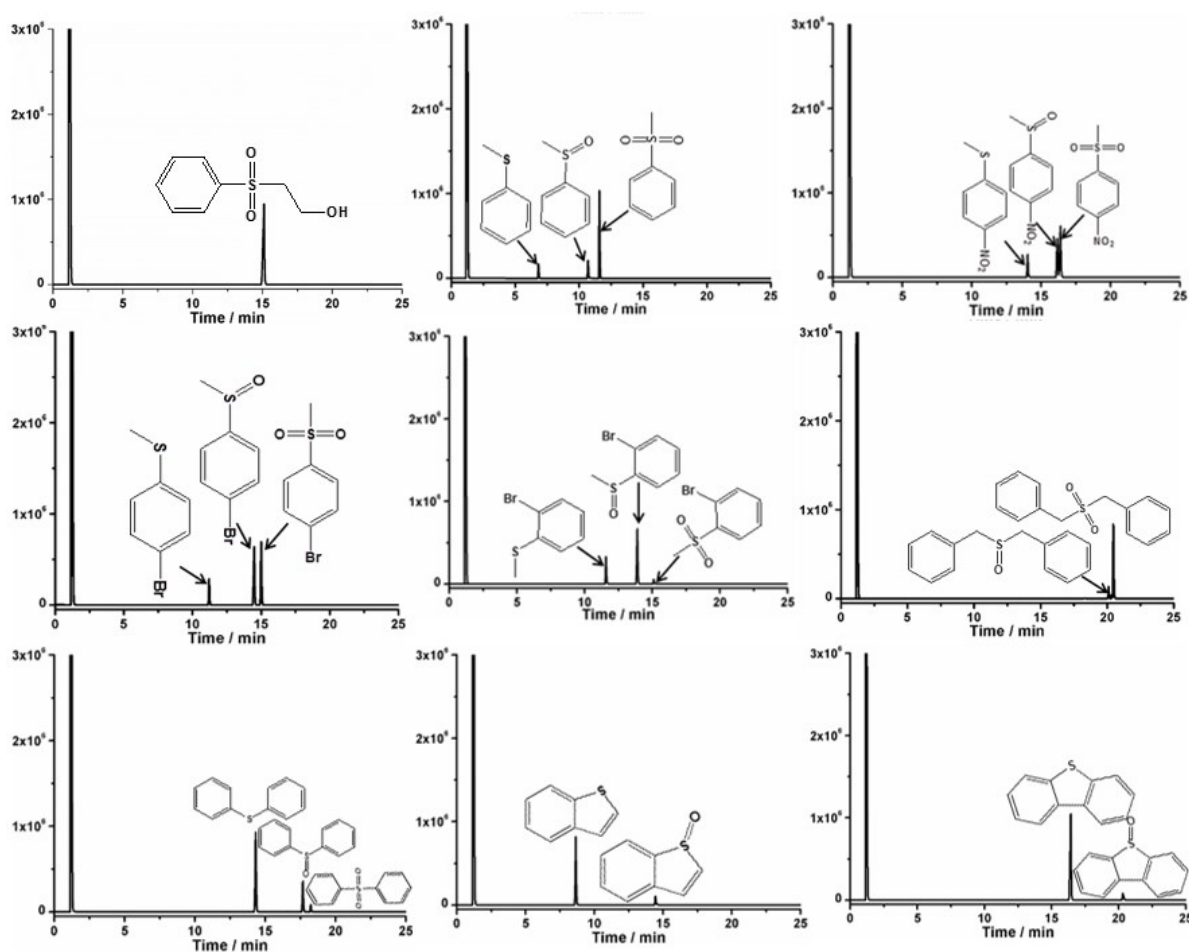


Fig S16. GC trace of the catalytic results for oxidation of entries 1 and 3-10. Reactions conditions: entries 1 and 3-10 (0.5 mmol), 30% H₂O₂ (1.5 mmol), and catalyst **2** (2.5 μmol) in CH₃CN (6 mL) at 80 °C, 3h.

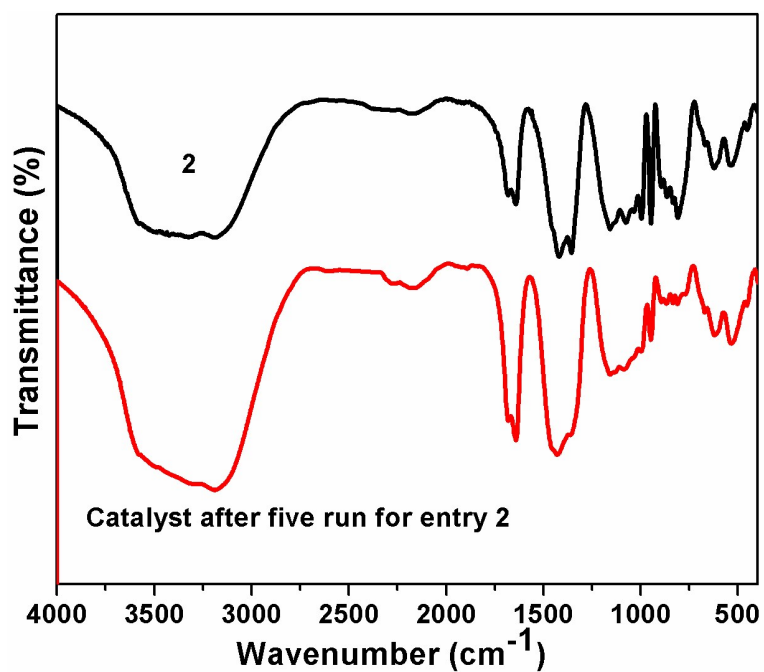


Fig S17. Comparison of IR spectra of the fresh catalyst and the recovered catalyst after the fifth-run catalytic reaction in entry 2.

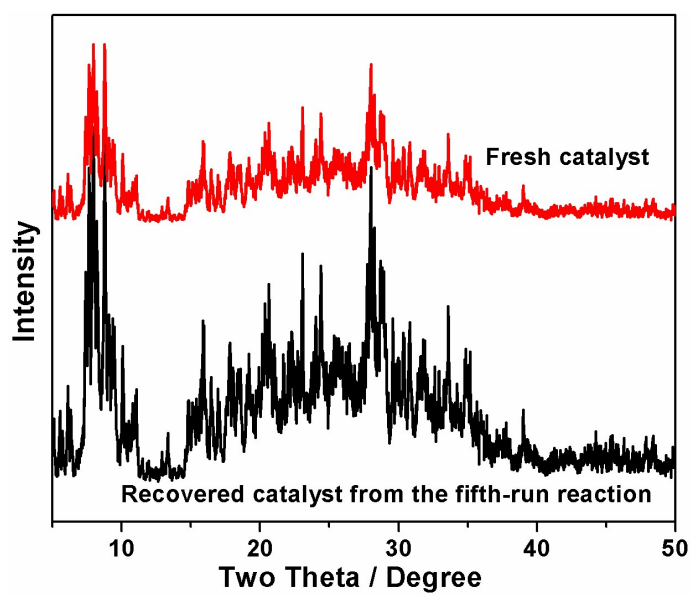


Fig. S18 Comparison of PXRD patterns of the fresh catalyst and the recovered catalyst after the fifth-run catalytic reaction in entry 2.